In-body Path Loss Model for Homogeneous Human Tissues

Divya Kurup, Wout Joseph, Günter Vermeeren, and Luc Martens

IBBT-Ghent University, Dept. of Information Technology

Gaston Crommenlaan 8 box 201, B-9050 Ghent, Belgium

Fax: +32 9 33 14899, E-mail: divya.kurup@intec.UGent.be

Abstract

A wireless body area network (WBAN) consists of a wireless network with devices placed close to, attached on, or implanted into the human body. Wireless communication within human body experiences loss in the form of attenuation and absorption. A path loss model is thus necessary to identify these losses in homogeneous medium which is proposed in this paper. The model is based on 3D electromagnetic simulations and is validated with measurements. Simulations are further extended for different relative permittivity ϵ_r and conductivity σ combinations spanning a range of human tissues at 2.45 GHz, and the influence of the dielectric properties on path loss is investigated and modeled. This model is valid for insulated dipole antennas separated by a distance up to 8 cm. Further, path loss in homogeneous medium is also compared with the path loss in heterogeneous tissues. The path loss model for homogeneous medium is the first in-body model as a function of ϵ_r, σ, and separation between antennas and can be used to design an in-body communication system.

Index Terms

Wireless body area networks (WBAN), Homogeneous medium, Heterogeneous medium, Path loss model, Insulation, Dipole antenna, Simulations, Measurements

I. Introduction

A wireless body area network (WBAN) is a network, consisting of nodes that communicate wirelessly and are located on or in the body of a person. These nodes form a network that extends over the body of a person. Depending on the implementation, the nodes consist of sensors and actuators, placed in a star or multihop topology [1].

Applications of WBANs include medicine, sports, military, and multimedia which utilizes the freedom of movement provided by the WBAN. As a WBAN facilitates unconstrained movement amongst users, it has brought a revolutionary change in patient monitoring and health care facilities. Active implants placed within the human body lead to better and faster diagnosis thus improving the quality of life of the patient. The PL model developed in this paper focuses on deep tissue implants such as endoscopy capsule. In such an application the implants go deep inside the body, which we have selected up to a distance of 8 cm. A PL model will help in understanding the influence of the dielectric properties of the surrounding tissues and the power attenuation of such implants.

Knowledge of the electromagnetic fields of active implants in the body is important for electromagnetic compatibility (EMC) studies, for the design of antennas in dielectric media, and for assessing potential health effects of electromagnetic radiation. The degree to which antennas can communicate with each other in a medium, characterized using the concept of path loss, is an important aspect of EMC research.The human body is a lossy medium, hence waves propagating from the transmitter are attenuated considerably before they reach the receiver. A path loss (PL) model helps to design optimum communication between nodes placed within or on the human body. To our knowledge there is very limited literature on propagation loss within the human body. In [2], initial results of an in-body propagation model in saline water is presented.Inaccuracies lead to large maximum deviations of 9 dB between the measurements and simulations. [2] considers a non-insulated hertzian dipole, hence the PL model can be applied only to very small dipole antennas. [3] provides various scenarios for channel modeling but does not provide a model for path loss. [4] discusses a link budget for an implanted cavity slot antenna at 2.45 GHz.

However, no model for various human tissues is suggested that can be used for path loss simulation. [5] discusses how standard antenna analysis techniques fail when antennas are in a conducting medium and emphasizes the determination of antenna gain in a conducting medium. However, it does not mention anything regarding path loss in the conducting medium.

The goal of this paper is to develop an empirical PL model for various homogeneous human tissues that describes the relationships between the PL and the relative permittivity ϵ_r and the conductivity σ of the human tissues, the distance between the antennas and the power attenuation. We also compare the PL in homogeneous medium with the PL in heterogeneous medium and explain the relationship between them. Simulations and measurements are performed at 2.457 GHz in the license free industrial, scientific and medical (ISM) band. This frequency band is chosen as there are no licensing issues in this band and higher frequency allows the use of a smaller antenna. First we perform measurements and simulations in homogeneous human muscle tissue. To validate the simulations with measurement, we use a flat phantom [6] filled with human muscle simulating liquid. After validating the simulations with measurements in human muscle tissue, simulations are extended over a broad range of ϵ_r and σ representing various homogeneous human tissues to calculate the PL. The PL thus obtained is used to propose a PL model applicable for the various homogeneous tissues in a human body.

As it is difficult for the manufacturers to test their system on actual humans, the proposed model can be used by them to evaluate the performance of in-body WBAN systems using well specified setups and to carry out link budget calculations. The path loss occurring in in-body is critical and the PL model can help to find out the maximum distance that can be covered between the Tx and the Rx within the body. Thus this model can be used for the in-body part of the link budget.

The outline of this paper is as follows. In Section II, the simulation and measurement setups are discussed. Section III discusses the results including the reflection coefficient and the path loss of the insulated dipole in human muscle tissue medium. The influence of ϵ_r and σ on path loss, the path loss model, and the validation of the models are presented in Section IV. Section V presents the PL in

hetereogeneous medium and finally, Section VI presents the conclusions.

II. Homogeneous Human Tissues: Method

A. Setup for One Type of Tissue : Human Muscle Tissue

We first investigate wave propagation at 2.457 GHz in human muscle tissue (relative permittivity $\epsilon_r = 50.8$ and conductivity $\sigma = 2.01$ S/m [7]) using measurements and simulations for insulated dipoles. After validation of the simulations and measurements for human muscle tissue, simulations are further extended for a broad range of homogeneous human tissues which is discussed in Section II-B. We develop two identical insulated dipoles (Fig. 1) for measurements where the dipole arms are perfect electric conductors (PEC) surrounded with an insulation made of polytetrafluoroethylene ($\epsilon_r = 2.07$ and $\sigma = 0$ S/m). We use dipole antennas for our study as they are the best understood antennas in free space and have a simple structure. Resonance is obtained for the insulated dipole antennas developed for measurements at a length ℓ_1 = 3.9 cm, for a frequency of 2.457 GHz. The resonance appears when the antenna is about equal to half the wavelength in a homogeneous medium equivalent to the combination of the insulation and the muscle tissue medium. Hence λ_{res} = 7.8 cm (where λ_{res} is the wavelength at which resonance occurs) and we can derive the equivalent permittivity $\epsilon_{r,equiv} = 2.45$ which is closer to the permittivity of the insulation than to the muscle tissue. The dipole arms have a diameter t_1 = 1 mm and the diameter of the insulation is t_2 = 5 mm. We use these dimensions in order to model the insulated dipole antennas in the simulation tools. Insulated dipoles are selected instead of bare dipoles because the insulation prevents the leakage of conducting charges from the dipole and reduces the sensitivity of the entire distribution of current to the electrical properties of the ambient medium. This property makes insulated dipoles valuable for WBAN purposes [8], [9].

1) Measurements: Measurements are executed using a vector network analyzer NWA (Rohde & Schwarz ZVR) and the scattering parameters $|S_{11}|_{\mathrm{dB}}$ and $|S_{21}|_{\mathrm{dB}}$ (with respect to 50 Ω) between Tx and Rx for the different separations are determined. The path loss is then calculated from $|S_{21}|_{\mathrm{dB}}$ as shown in

Section III-C. A flat phantom, representing the trunk of a human body and recommended by CENELEC standard EN50383 [6] (dimensions $80\times50\times20$ cm^3), is filled with muscle tissue simulating fluid (relative permittivity $\epsilon_r = 50.8$ and conductivity $\sigma = 2.01$ S/m at 2.45 GHz [7]). The insulated dipoles used in the measurements are shown in Fig. 1, with the insulated dipole antenna connected to the NWA using a coaxial cable. The two insulated dipoles are immersed, placed parallel and lined up for maximal power transfer at 5 cm above the bottom of the flat phantom (Fig. 2). A robot (3D-positioning Phytron IXEα-C-T) with an accuracy of 0.025 mm is used to position the Tx and the Rx in the human muscle tissue simulating fluid. The Tx is fixed inside the fluid and the Rx is moved by means of the robot arm. The measurements are performed every 2 mm starting from 6 mm up to 8 cm. We start from 6 mm as this is the closest distance at which we could place both the antennas using the robotic arm.

2) Simulations: Simulations are performed using a 3D electromagnetic solver SEMCAD-X (SPEAG, Switzerland), a finite-difference time-domain (FDTD) program and FEKO (EMSS, South Africa), a method of moments (MoM) program. SEMCAD-X enables non-uniform gridding. The maximum grid step in the muscle tissue medium is 1 mm at 2.457 GHz. The flat phantom is modeled according to [6]. Simulations in FEKO also use the exact dimensions of the insulated dipoles placed in the muscle tissue medium. For accurate modeling in the MoM tool, segmentation rules are adhered to (segment length = λ_{res}/12, edge length = λ_{res}/12). In both simulations a voltage source is used, which is placed in the gap between the two dipole arms as shown in Fig. 1. Simulations are carried out starting at d = 6 mm from the transmitting antenna up to a distance of 8 cm.

B. Setup for All Human Tissues

To determine the influence of ϵ_r and σ on PL, simulations are carried out using the insulated dipole antenna of Section II-A for a range of ϵ_r and σ and PL is determined. ϵ_r is varied from $5 \leq \epsilon_r \leq 65$ and σ from 0.5 S/m $\leq \sigma \leq$ 3.5 S/m. This range is chosen because most human tissues at 2.45 GHz are characterized by an ϵ_r and σ in this range [10]. The simulations of the combination of ϵ_r and σ are carried out from 6 mm up to a distance of 8 cm using the MoM program. MoM program is used as

simulations using this program are faster than the FDTD program. The setup is the same as mentioned in the Section II-A2. In FEKO we use a current source because of the use of the finite element method (FEM). A total of 1547 simulations were carried to obtain the return loss and PL as a function of distance d, σ, and ϵ_r.

III. Results : Human Muscle Tissue

A. Return Loss for a Single Insulated Dipole

The measured and simulated reflection losses of the insulated dipole in human muscle tissue as a function of frequency are compared in Fig. 3. The agreement obtained between the measured and the simulated insulated dipoles at 2.457 GHz is acceptable. The simulated and the measured dipoles are well matched radiators in human muscle tissue. The $|S_{11}|_{\mathrm{dB}}$ for the insulated dipoles at 2.457 GHz is -13.60 dB, -12.29 dB, and -11.25 dB for the measurements, FDTD, and MoM tool respectively. Differences in the $|S_{11}|_{\mathrm{dB}}$ between the two simulation tools can be attributed to the inherent different modeling techniques.

B. Influence of Thickness of Insulation on the Resonance Frequency

In this section the influence of the insulation thickness t on the resonance frequency is studied. We define t as $(\frac{t_2-t_1}{2})$ where t_2 is the diameter of the insulation and t_1 is the diameter of the dipole (PEC) (See.Fig. 2). The influence of t from 0.1 mm up to 4.5 mm is studied. We define resonance frequency as the frequency where the imaginary part of the input impedance is zero [11]. Fig. 4 shows that an increase in thickness of the insulation causes the resonance frequency to increase. Hence the length of the insulated antenna as well as the thickness of the insulation have an effect on the resonance frequency of the antenna. t of 0.4 mm causes the antenna to resonate at a lower frequency of 1.31 GHz than that with a thickness of 1 mm resulting in a resonance frequency of 1.86 GHz (Fig. 4). As t increases, the $\epsilon_{r,equiv}$ of the insulation and the medium decreases and the $\epsilon_{r,equiv}$ will become closer to the value of the permittivity of the insulator. Thus, when t increases the resonance frequency will increase which can be seen in Fig. 4. In order to achieve a certain resonance frequency for the antenna varying the insulation thickness can

be considered as an option. Fig. 5 shows that the -10 dB bandwidth (BW) of $|S_{11}|_{\mathrm{dB}}$ as a function of t is large enough to cover the whole of the ISM band at 2.45 GHz for our configuration which has an insulation thickness of 4.5 mm. The insulated dipole antenna is best matched for t = 1 mm, however with a t = 4.5 mm we have an antenna that operates in the ISM band.

C. Path Loss

PL is defined as the ratio of input power at port 1 (P_{in}) to power received at port 2 (P_{rec}) in a two-port setup. PL in terms of transmission coefficient is defined as $1/|S_{21}|^2$ with respect to 50 Ω when the generator at the Tx has an output impedance of 50 Ω and the Rx is terminated with 50 Ω. This allows us to regard the setup as a two-port circuit for which we determine $|S_{21}|_{\mathrm{dB}}$ with reference impedances of 50 Ω at both ports:

$$PL|_{\mathrm{dB}} = (P_{in}/P_{rec}) = -10\ \log_{10}|S_{21}|^2 = -|S_{21}|_{\mathrm{dB}}, \tag{1}$$

Fig. 6 shows the simulated and measured PL in human muscle tissue as a function of distance d for the insulated dipole. The measured and the simulated values show excellent agreement up to 8 cm. The deviations between the measurements and the simulations are very low: with SEMCAD-X, the maximal and average deviation up to 8 cm are 1.7 dB and 0.8 dB, respectively, and for FEKO the maximal and average deviation are 3.4 dB and 1.3 dB, respectively.

1) PL Model: In this section the measurement results are used to develop a PL model as a function of distance in human muscle tissue at 2.457 GHz. The measurements and the fitted model in human muscle tissue are shown in Fig. 6. The PL is modeled as follows :

$$PL|_{\mathrm{dB}} = (10\ \log_{10} e^2)\ \alpha_1\ d + C_1|_{\mathrm{dB}} \qquad for\ d \leq d_{bp}, \tag{2}$$

$$PL|_{\mathrm{dB}} = (10\ \log_{10} e^2)\ \alpha_2\ d + C_2|_{\mathrm{dB}} \qquad for\ d \geq d_{bp}, \tag{3}$$

where the parameters α_1 and α_2 are the attenuation constants [$\frac{1}{cm}$], $C_1|_{\mathrm{dB}}$ and $C_2|_{\mathrm{dB}}$ are constants, d_{bp} = 2.78 cm is the breakpoint where the mutual coupling between the transmitter and the receiver

ends, and d is in cm. The model consists of two regions : *Region 1* and *Region 2*. *Region 1*, $d \leq d_{bp}$ is defined as the region which is very close to the Tx dipole and extends from 0 cm to 2.78 cm. Here the Tx and the Rx are close to each other and this causes the antennas to interact with each other and alter the impedances due to mutual coupling. In *Region 2*, $d \geq d_{bp}$, the mutual coupling between the Tx and the Rx disappears. We observe that the input impedance of the Tx keeps changing up to a certain separation between the Tx and the Rx, after which the input impedance becomes constant. This variation in the input impedance due to mutual coupling ceases to exist after the d_{bp}.The parameter values in (2) and (3) are obtained by using a least square-error method and are shown in Table I [9].

IV. Influence of ϵ_r and σ of human tissues on path loss

A. Resonance frequency as a function of ϵ_r and σ

1) ϵ_r : In this section the resonance frequency of the insulated dipole as a function of ϵ_r is determined. As the antenna is placed in medium with a range of ϵ_r, the resonant frequency is determined by the $\epsilon_{r,equiv}$ of the insulation and the medium. Thus Fig. 7 shows the equivalent permittivity $\epsilon_{r,equiv}$ for the range of ϵ_r as a function of resonance frequency. In the Fig. 7 the $\epsilon_{r,equiv}$ = 2.82 corresponds to ϵ_r = 5 and $\epsilon_{r,equiv}$ = 3.85 corresponds to ϵ_r = 60. The resonance frequency of the antenna increases, e.g, at $\epsilon_{r,equiv}$ = 3.82 the resonance frequency is 1.93 GHz while at $\epsilon_{r,equiv}$ = 3.22 the resonance frequency is 2.13 GHz. Thus as $\epsilon_{r,equiv}$ increases the resonance frequency decreases.

2) σ: In this section the resonance frequency of the insulated dipole as a function of σ is determined. At ϵ_r = 50.8 and σ varying from 0.5 to 3.5 S/m the resonance frequency shifts only from 2.24 GHz to 2.17 GHz which is limited. Hence, the resonance frequency is not significantly affected by the conductivity of the medium.

B. Path loss model as a function of ϵ_r and σ

PL as a function of distance for a range of σ and ϵ_r ($5 \leq \epsilon_r \leq 65$, 0.5 S/m $\leq \sigma \leq$ 3.5 S/m, see Section II-B) at frequency of 2.45 GHz is discussed in this section. For example, Fig. 8 shows PL as a

function of distance for a range of σ and ϵ_r = 50. As conductivity introduces losses, PL increases with increasing conductivity. Fig. 9 shows PL as a function of distance for a range of ϵ_r with σ = 2 S/m. It can be seen that PL decreases with increasing permittivity. The insulated dipole is a better radiator at higher values of ϵ_r as for our configuration we have an antenna that resonates for an ϵ_r = 50.8. In Section IV-B1 we discuss the dependency of the attenuation constant α on ϵ_r which will help us further in understanding the decrease in PL with increase in ϵ_r. The simulated PL results for the range of ϵ_r and σ are now used to develop a PL model as a function of d, ϵ_r, and σ at 2.457 GHz. We apply the PL model of (2) and (3) for the considered ranges of ϵ_r and σ. Using the PL model of (2) and (3) we obtain the attenuation constants α_1, α_2, the constants $C_1|_{\mathrm{dB}}$, $C_2|_{\mathrm{dB}}$, and d_{bp} for the range of the dielectric parameters.

1) Attenuation constant model: In this section the simulation results over the range of ϵ_r and σ are used to develop an attenuation constant model with the attenuation constants α_1 and α_2 as a function of ϵ_r and σ at 2.457 GHz. The attenuation constants α_1 and α_2 are derived using (2) and (3). Fig. 10 shows that the attenuation constant α_1 increases with increasing value of σ. The same is observed for the attenuation constant α_2 which increases for increasing value of σ. Hence PL increases for higher σ. The values of both α_1 and α_2 are maximal for the minimum value of ϵ_r. The attenuation constants vary exponentially with respect to ϵ_r and linearly with respect to σ. This can be explained as follows. For plane waves the following equation for the attenuation constant α in a lossy medium is defined [12]:

$$\alpha = \omega \left[\left(\frac{\mu\epsilon}{2} \right) \left(\sqrt{(1 + \frac{\sigma^2}{\epsilon^2\omega^2}} - 1 \right) \right]^{1/2} \qquad \left[\frac{Nep}{m} \right], \tag{4}$$

where α = the attenuation constant, $\omega = 2 \cdot \pi \cdot f$ = angular frequency [rad/sec], f= frequency = 2.45 GHz, μ = permeability of the lossy medium, $\epsilon = \epsilon_r\epsilon_0$, ϵ_r= permittivity of the lossy medium, and σ = conductivity of the lossy medium [S/m]. For muscle tissue we have σ = 2.01 S/m and ϵ_r = 50.8, hence we can conclude that $\frac{\sigma^2}{\epsilon^2\omega^2} << 1$ and thus only the displacement current exists. Thus the approximation of the attenuation factor becomes

$$\alpha = \frac{\sigma}{2}\sqrt{\frac{\mu}{\epsilon}} \qquad \left[\frac{Nep}{m} \right], \tag{5}$$

From (5) we conclude that the attenuation is directly proportional to the conductivity of the medium σ and we observe that the attenuation constant varies linearly in the simulated results. The attenuation constant is inversely proportional to the square root of the permittivity of the medium ϵ_r thus validating our observation in the simulation results. Due to this PL increases with increasing σ and PL decreases with increasing ϵ_r. For α_2 we obtain a value of 0.66 [1/cm] and when we calculate the value of α_2 using (4) or (5) at ϵ_r = 50.8 and σ= 2.01 [S/m] we obtain a value of 0.52 [1/cm]. This shows the correctness of the models and the fit shown in (2) and (3) Therefore we propose the following models for α_1 and α_2:

$$\alpha_1 = (A_1 e^{(B_1 \epsilon_r)} + D_1) \cdot (E_1\ \sigma + F_1) \qquad for\ d \leq d_{bp}, \tag{6}$$

$$\alpha_2 = (A_2 e^{(B_2 \epsilon_r)} + D_2) \cdot (E_2\ \sigma + F_2) \qquad for\ d \geq d_{bp}, \tag{7}$$

with the values of the constants A_1, A_2, B_1, B_2, E_1, E_2, F_1, and F_2 provided in the Table II. From Table II it can be seen that the model of (6) and model of (7) have good agreement with the simulation results and the relative error is 3.9 % and 3.5 %.

From the analysis the worst-case tissue properties (i.e., resulting in highest PL) can also be obtained. It is found that the PL is maximal for a tissue with the highest σ and the lowest ϵ_r. The small intestine has been identified as having the worst-case tissue properties with a high σ = 3.17 S/m and ϵ_r= 54.42.

2) Model for the constant C: Fig. 11 shows the constant C_1 with the fit as a function of both ϵ_r and σ. The trend of the constant C_2 is similar to C_1 as shown in Fig. 11. The constants C_1 and C_2 are fit using the following :

$$C_1|_{\mathrm{dB}} = (U_1 e^{(V_1/\epsilon_r)} + W_1) \cdot (X_1\ \sigma + Y_1) \qquad for\ d \leq d_{bp}, \tag{8}$$

$$C_2|_{\mathrm{dB}} = (U_2 e^{(V_2/\epsilon_r)} + W_2) \cdot (X_2\ \sigma + Y_2) \qquad for\ d \geq d_{bp}, \tag{9}$$

with the values of the constants U_1, U_2, V_1, V_2, W_1, W_2, X_1, X_2, Y_1 and Y_2 provided in the Table III. The constants C_1 and C_2 increase with an increase in ϵ_r, while the constants C_1 and C_2 decrease with an increase in σ. The error between the model of (8) and the model of (9) and the simulation results is

0.52 dB and 0.33 dB, respectively. The low error shows very good agreement between the models and the simulation results.

3) Break point d_{bp} : In order to obtain the PL model using (2) and (3) the break points are selected. The break point d_{bp} is defined at a distance where the coupling between the transmitter and the receiving antenna ends. Fig. 12 shows an example of $|Z_{in}|$ versus distance, where $|Z_{in}|$ is the magnitude of the input impedance of the transmitting antenna at σ = 2.0 S/m over the range of ϵ_r. The distance where the transition from Region 1 to Region 2 occurs (i.e., d_{bp}) can be clearly seen from the Fig. 12 with the variation of $|Z_{in}|$. Similar results are obtained over the range of σ. We select the d_{bp} such that it is 5 % of the maximum deviation between the input impedance at all distances and the input impedance at 8 cm which we consider as the constant value. The break point is deduced for the PL model for the combinations of ϵ_r and σ. It is seen that d_{bp} decreases as σ increases. As σ increases, higher losses are introduced due to which the coupling only exists for smaller distances, hence d_{bp} decreases. We observe that d_{bp} increases with increase in ϵ_r. As the PL decreases with an increase in ϵ_r we can deduce that at higher ϵ_r coupling exists over a larger distance between the transmitting and the receiving antenna.

We develop a model for the d_{bp} as a function of ϵ_r and σ.

$$d_{bp}(\epsilon_r, \sigma) = (Pe^{(Q\epsilon_r)}) \cdot (Re^{-(S\sigma)} + T). \tag{10}$$

Thus the break point increases with an increase in ϵ_r and decreases with an increase in σ. P, Q, R, S, and T are constants here and their values can be found in Table IV.

4) Error in the model: In Section IV-B2 and Section IV-B1 we have obtained models for the attenuation constant α and the constant C. In this section we validate the models obtained by comparing them with the PL obtained in the simulation, i.e, (2) and (3). We rewrite (2) and (3) as follows :

$$PL|_{\text{dB}} = (10\ \log_{10} e^2)\ (A_1 e^{(B_1\epsilon_r)} + D_1) \cdot (E_1\ \sigma + F_1)\ d + (U_1 e^{(V_1/\epsilon_r)} + W_1) \cdot (X_1\ \sigma + Y_1) \quad for\ d \leq d_{bp}(\epsilon_r, \sigma), \tag{11}$$

$$PL|_{\mathrm{dB}} = (10\ \log_{10} e^2)\ (A_2 e^{(B_2 \epsilon_r)} + D_2) \cdot (E_2\ \sigma + F_2)\ d + (U_2 e^{(V_2/\epsilon_r)} + W_2) \cdot (X_2\ \sigma + Y_2) \qquad for\ d \geq d_{bp}(\epsilon_r, \sigma). \tag{12}$$

The mean deviation from the models is only 0.83 dB and the maximum mean deviation is 2.56 dB for the entire range of permittivity ($5 \leq \epsilon_r \leq 65$) and conductivity(0.5 S/m $\leq \sigma \leq$ 3.5 S/m), with a total combination of 1547 simulations, which is very good. Low values of deviations show excellent agreement between the general PL models of (11) and (12) and the simulation results.

V. Heterogeneous Medium: Path Loss

A. Setup and Configuration

PL in heterogeneous medium is investigated using an enhanced anatomical model of a 6 year male child from the $Virtual\ Family$ [13]. The model is based on magnetic resonance images (MRI) of healthy volunteers. The male child model (virtual family boy, VFB) has a height of 1.17 m and a weight of 19.5 kg. The model consists of 81 different tissues. The dielectric properties of the body tissues have been taken from the Gabriel database [10]. Simulations to determine PL are carried out using FDTD technique in SEMCAD-X. Insulated dipole antennas are placed in the trunk of the male child model to determine PL from a distance of 6 mm up to 120 mm for application such as an endoscopy capsule. Since the simulation using the whole body of the male child model consumes a lot of time, the simulation domain is reduced to just cover the trunk of the male child model. We select the male child model as capsule endoscopy is used as a tool for diagnosis for children with evidence of internal bleeding and abdominal pain. Capsule endoscopy has been accepted in adults by many gastroenterologists, however its usage in children has lagged due to the belief by pediatricians that the pills are too large to be swallowed by children [14], [15]. However, reports do suggest that children as young as two and a half years old are successfully undergoing capsule endoscopy [16]. The insulated dipole antennas are placed such that the Tx lies in the stomach and the Rx moves from 0.6 cm to 4 cm through the stomach (ϵ_r = 62.16 and σ = 2.21 S/m) , and

then moves partially into the liver (ϵ_r = 54.81 and σ = 2.25 S/m) starting from 5 cm and and then entirely up to 12 cm. This is a theoretical approach in order to study the influence of heterogeneous tissues on the PL.

B. PL in heterogeneous medium

Fig. 13 shows PL in the heterogeneous medium with a separation between the insulated dipole antennas up to 12 cm and the comparison with the PL in homogeneous medium having dielectric properties of the liver and stomach. PL of the heterogeneous medium shows a slight change in slope at distances where the Rx antenna makes a transition from one medium to the other (at 5 cm) in Fig. 13 which is due to change in the dielectric property of the tissues and thus due to the difference in the attenuation constant for each tissue through which the antenna traverses. For a heterogeneous medium the attenuation constant obtained by using the PL model will be an effective attenuation constant which will take into consideration the different tissues through which the wave propagates. Thus the attenuation constant from the homogeneous PL model will be replaced by an effective attenuation constant in case of a heterogeneous medium.

PL in heterogeneous medium from a distance of 0.6 cm to 4 cm is in the stomach and hence it is compared to the PL in homogeneous medium with dielectric property of the stomach (ϵ_r = 62.16 and σ = 2.21 S/m): it can be observed that the PL of both are similar and follow the same trend. The PL in heterogeneous medium from a distance of 5 cm to 12 cm is in the liver and hence it is compared to the PL in homogeneous medium with dielectric properties (ϵ_r = 54.81 and σ = 2.25 S/m) which also shows the same trend. In Fig. 13 PL in heterogeneous human model is in between the PL of the homogeneous tissues and lower than the PL in worst-case realistic tissue which is the small intestine (ϵ_r= 54.42 and σ = 3.17 S/m), (Section IV-B1).

The deviation between the PL in heterogeneous human model and homogeneous human tissues can be attributed to various parameters that need to be considered in a heterogeneous medium for e.g., proximity of different tissue layers, and the transition of the whole antenna to another tissue does not take place immediately but the antenna moves into the next tissue part by part.

VI. Conclusion

We thus demonstrate for the first time the influence of ϵ_r and σ of the various tissues on the PL and the PL model, thus providing a better understanding of PL in different tissues. For the first time an extensive PL study has been performed using insulated dipoles within various homogeneous lossy human tissues and an empirical PL model is developed that describes the relationships between the PL and the relative permittivity ϵ_r, the conductivity σ of the human tissues, and the distance between the antennas at 2.457 GHz. The mean error of C_1 and C_2 is 0.52 dB and 0.33 dB, respectively. The PL in homogeneous medium can also be used as a measure to understand the PL in heterogeneous medium. The proposed general path loss model is the first in-body model for varying values of ϵ_r, σ and distance and can be used by manufacturers to design an in-body communication system.

References

[1] B. Latre, G. Vermeeren, I. Moerman, L. Martens, S. D. F. Louagie, and P. Demeester, "Networking and propagation issues in body area networks," *IEEE 11th Symposium on Communications and Vehicular Technology in the Benelux 2004, SCVT 2004*, November 2004 (CD-ROM).

[2] S. K. S. Gupta, Y. Prakash, E. Elsharawy, and L. Schwiebert, "Towards a propagation model for wireless biomedical applications," *IEEE International Conference on Communications*, vol. 3, pp. 1993–1997, May 2003.

[3] A. Johansson, "Wireless communication with medical implants," Ph.D. dissertation, Lund University, 2004.

[4] K. Ito and Wei Xia and Masaharu Takahashi and K. Saito, "An Implanted Cavity Slot Antenna for Medical Communication Systems," in *3rd European Conference on Antennas and Propagation (EuCAP)*, Berlin, Germany, March 2009, pp. 718–721.

[5] R. Moore, "Effects of a surrounding conducting medium on antenna analysis," *Antennas and Propagation, IEEE Transactions*, vol. 11, pp. 216–225, 1963.

[6] CENELEC EN50383, "Basic standard for the calculation and measurement of electromagnetic field strength and SAR related to human exposure from radio base stations and fixed terminal stations for wireless telecommunication systems (110 MHz - 40 GHz)," Sept 2002.

[7] FCC OET Bulletin 65, Revised Supplement C, "Evaluating Compliance with FCC Guidelines for Human Exposure to Radiofrequency Electromagnetic Fields," Federal Communication Commission, Office of Engineering and Technology, June 2001.

[8] R. W. P. King, G. S. Smith, M. Owens, and T. T. Wu, *Antennas in matter fundamentals, theory and applications*. Cambridge, MA : MIT Press, 1981.

[9] D. Kurup, W. Joseph, G. Vermeeren, and L. Martens, "Path loss model for in-body communication in homogeneous human muscle tissue," *IET Electronics Letters*, pp. 453–454, April 2009.

[10] C. Gabriel and S. Gabriel., "Compilation of the dielectric properties of body tissues at RF and microwave frequencies," *[ONLINE] Available:http://www.brooks.af.mil/AFRL/HED/hedr/reports/dielectric/home.html*, Tech. Rep. AL/OE-RE-1996-0037,1996.

[11] K. Iizuka, "An experimental study of the insulated dipole antenna immersed in a conducting medium," *Antennas and Propagation, IEEE Transactions*, vol. 11, pp. 518–532, 1963.

[12] J. A. Stratton, *Electromagnetic Theory*. McGraw-Hill Book Company Inc., 1941.

[13] A.Christ, "The virtual family development of anatomical CAD models of two adults and two children for dosimetric simulations," *in preparation*.

[14] B. Barth, K. Donovan, and V. Fox, "Endoscopic placement of the capsule endoscope in children," *Gastrointestinal Endoscopy*, vol. 60, pp. 818–821, November 2004.

[15] E. Seidman and M. Dirks, "Capsule endoscopy in the pediatric patient," *Current Treatment Options Gastroenterol*, vol. 9, pp. 416–22, September 2006.

[16] H. Kavin, J. Berman, T. Martin, A. Feldman, and K. Forsey-Koukol, "Capsule endoscopy for a 2.5-year-old child: Obscure gastrointestinal bleeding from mixed, juvenile, capillary hemangioma-angiomatosis of the jejunum," *Pediatrics*, vol. 117, pp. 539–543, February 2006.

Authors' affiliations

Divya Kurup, Wout Joseph, Günter Vermeeren, and Luc Martens (Ghent University / IBBT, Dept. of Information Technology, Gaston Crommenlaan 8 box 201, B-9050 Ghent, Belgium, Fax: +32 9 33 14899, E-mail: divya.kurup@intec.UGent.be)

LIST OF TABLES

LIST OF FIGURES

TABLE I

PARAMETER VALUES AND STANDARD DEVIATIONS OF THE FITTED MODELS FOR PL_{dB} IN HUMAN MUSCLE TISSUE.

Parameter	$\alpha_i[\frac{1}{cm}]$	C_i[dB]	$Standard\ Deviation$[dB]	dev_{imax}[dB]	dev_{iavg}[dB]
$Model\ of\ (2)$	0.99	7.18	0.15	0.56	0.26
$Model\ of\ (3)$	0.66	15.79	0.28	1.22	0.40

TABLE II

PARAMETER VALUES OF THE ATTENUATION CONSTANT $|\alpha_i|$

Parameter	A_i	B_i	D_i	E_i	F_i	Relative Error [%]
$Model\ of\ (6)$	7.19	-0.04	4.86	0.05	0.05	3.9 %
$Model\ of\ (7)$	3.02	-0.04	1.83	0.11	0.07	3.5 %

TABLE III

PARAMETER VALUES OF THE CONSTANT $|C_i|$

Parameter	U_i	V_i	W_i	X_i	Y_i	σ_i[dB]
$Model\ of\ (8)$	1.98	-22.11	0.66	-1.05	6.56	0.52
$Model\ of\ (9)$	0.47	-28.59	0.55	-2.24	21.18	0.33

TABLE IV

PARAMETER VALUES OF THE BREAK POINT $|d_{bp}|$

Parameter	P_i	Q_i	R_i	S_i	T_i	Relative Error [%]
$Model\ of\ \|d_{bp}\|$	0.29	0.01	4.83	0.30	0.68	7.3 %

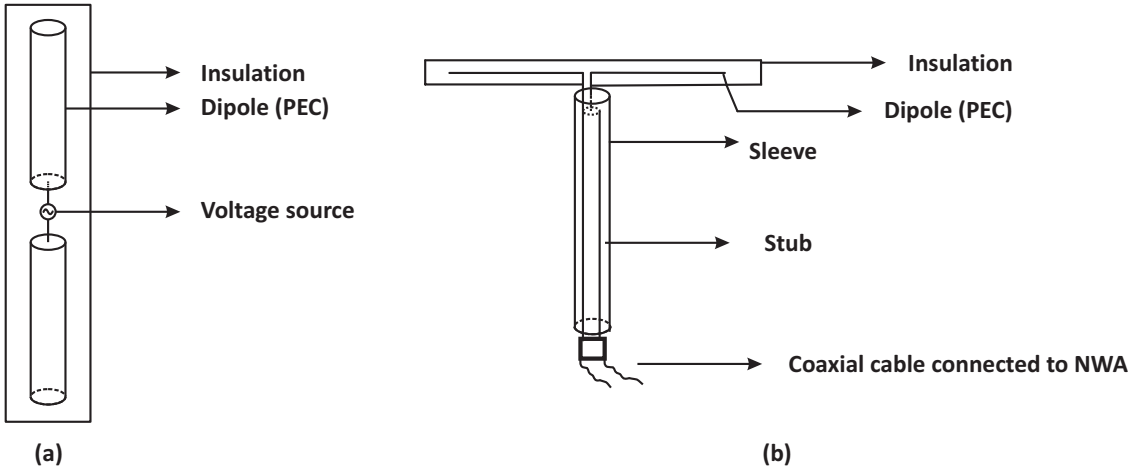

Fig. 1. Insulated dipole configuration (a) Simulation (b) Measurement

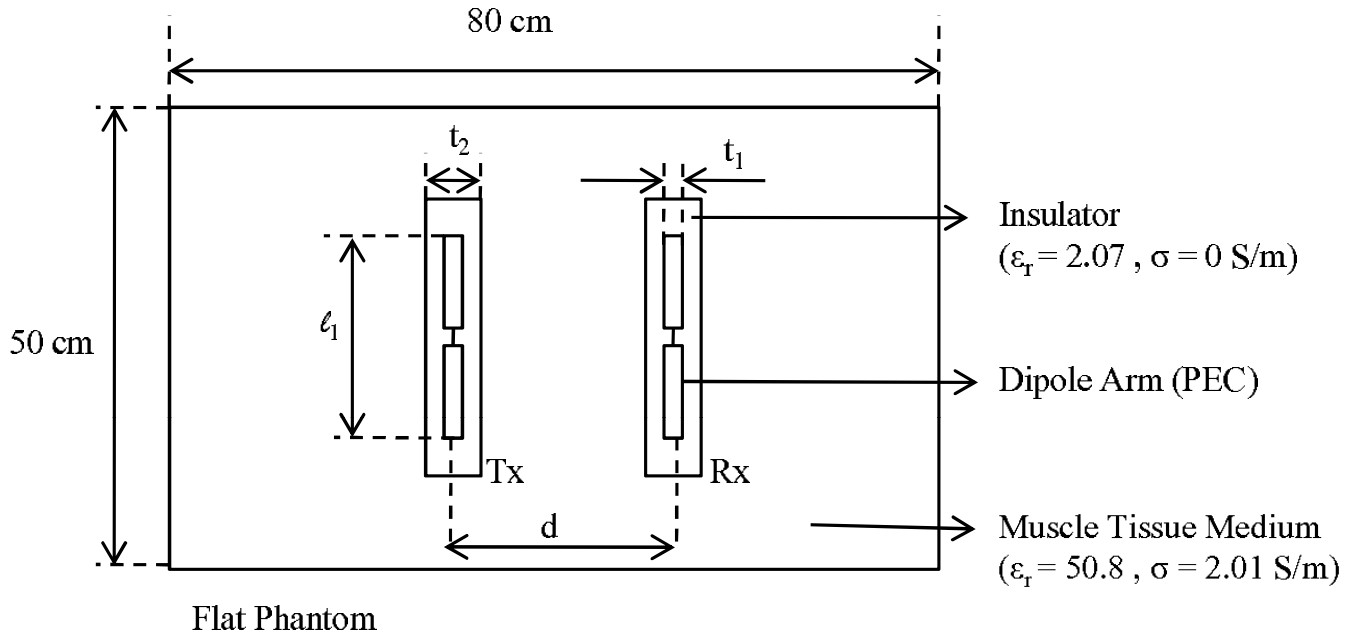

Fig. 2. Simulation setup and parameters.

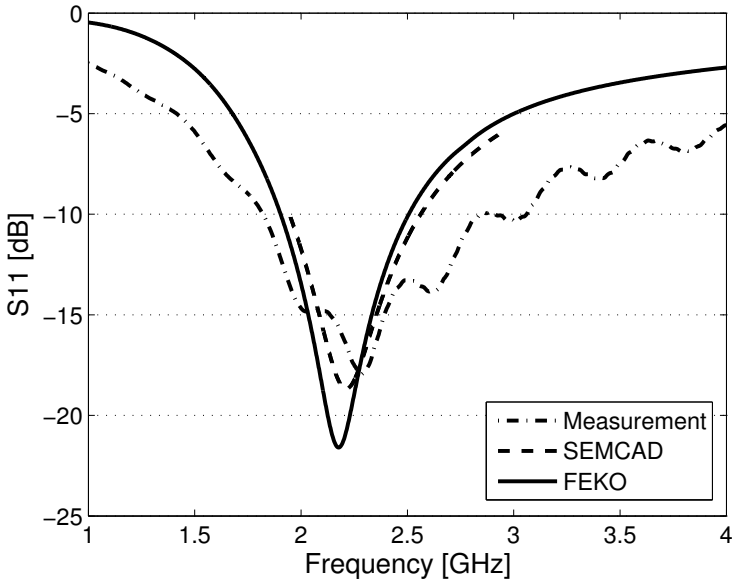

Fig. 3. Comparison between measured and simulated reflection loss of the insulated dipole in human muscle tissue.

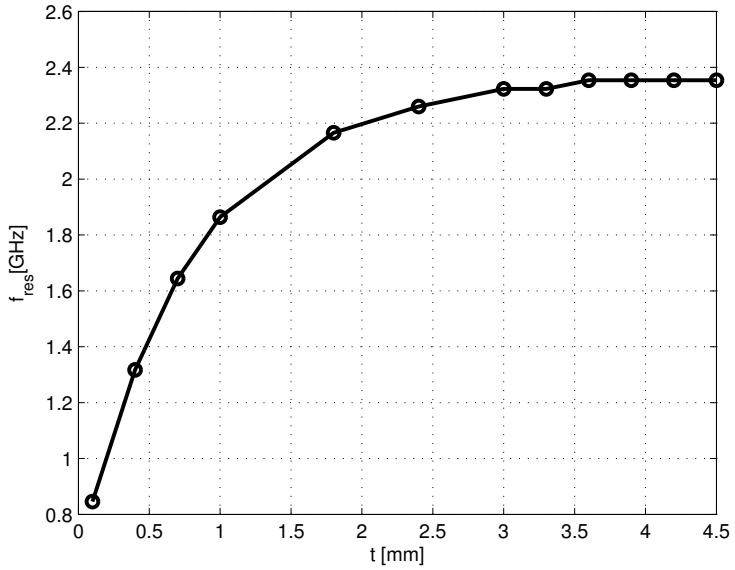

Fig. 4. Resonance frequency vs. insulation thickness of the insulated dipole.

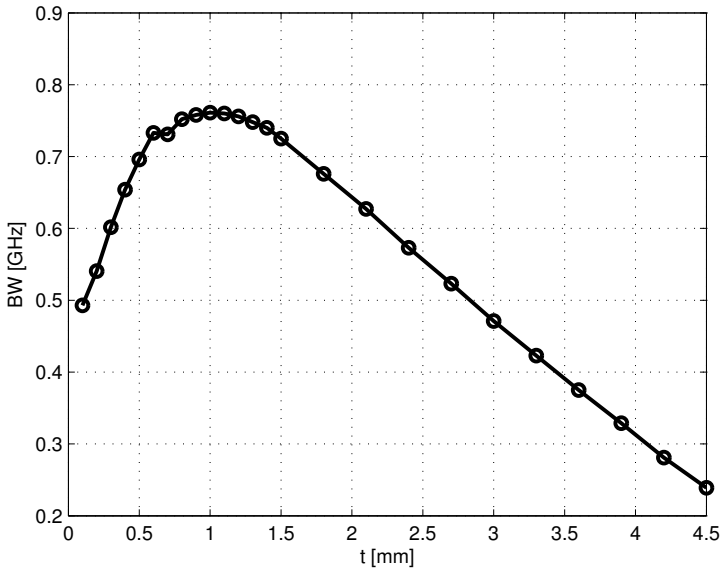

Fig. 5. -10 dB bandwidth of $|S_{11}|_{dB}$ vs. insulation thickness of the insulated dipole.

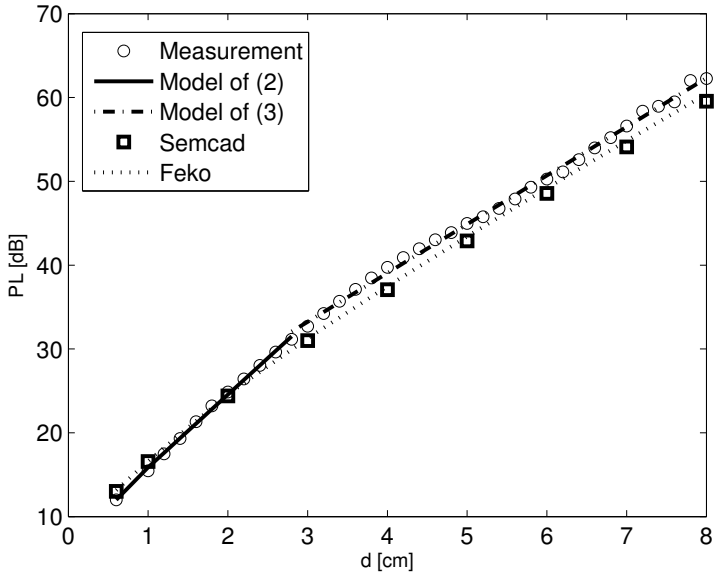

Fig. 6. Measured path loss, simulated path loss and fitted models as a function of separation between the Tx and the Rx.

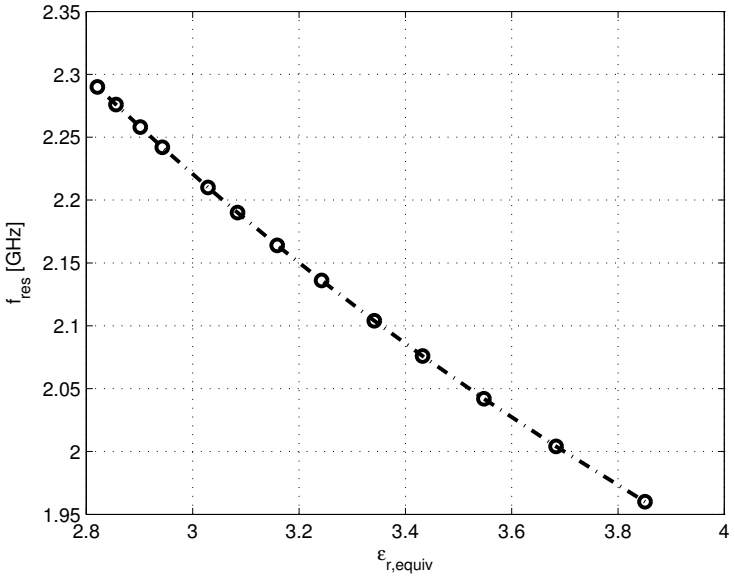

Fig. 7. Resonance frequency of the insulated dipole vs. $\epsilon_{r,equiv}$ (σ = 2.01 [S/m]).

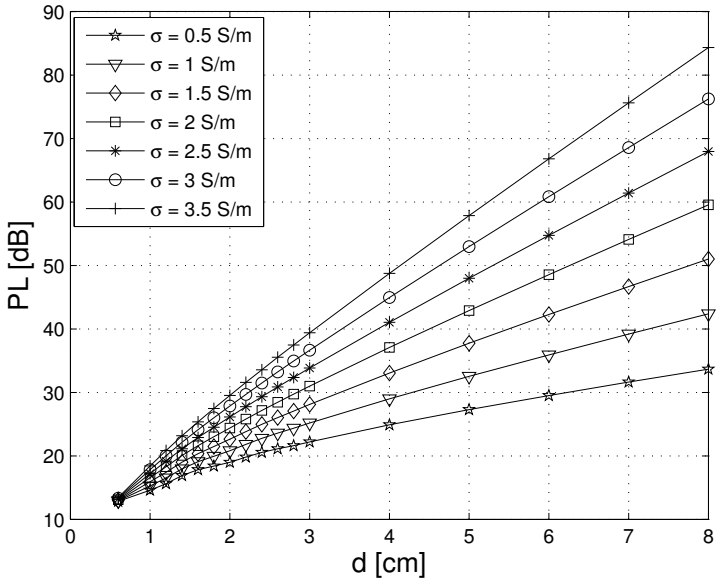

Fig. 8. Path loss vs. separation between the Tx and the Rx for σ (ϵ_r = 50).

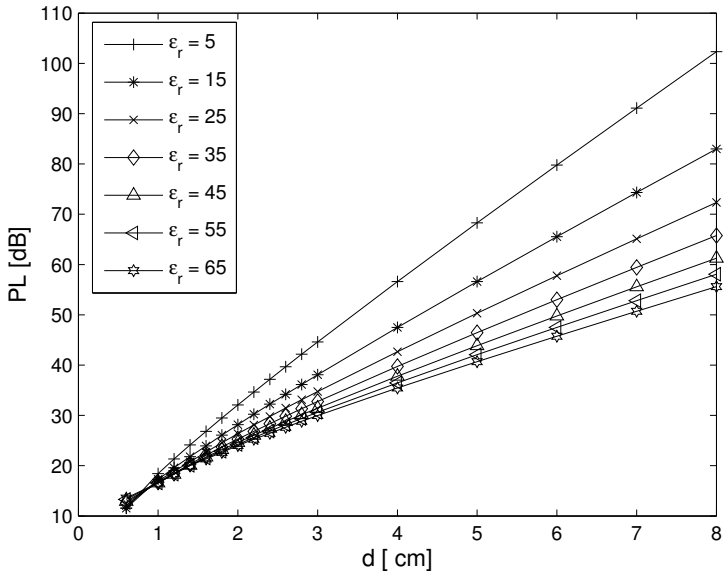

Fig. 9. Path loss vs. separation between the Tx and the Rx for ϵ_r (σ = 2 S/m).

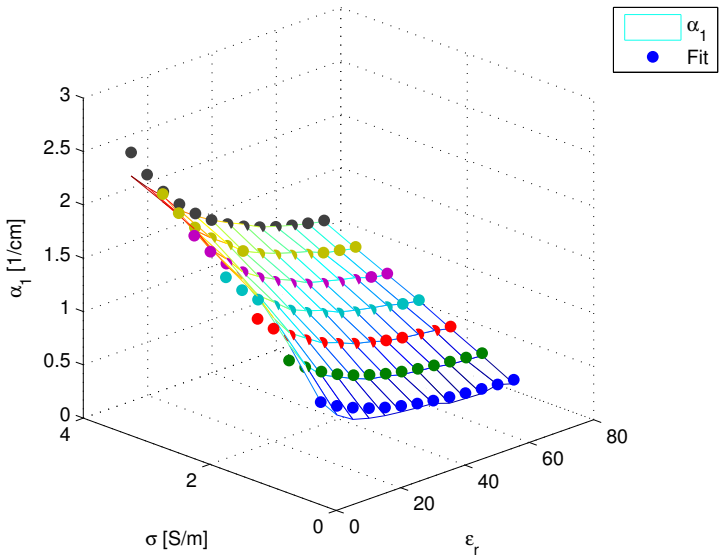

Fig. 10. Attenuation constant α_1 as a function of both ϵ_r and σ.

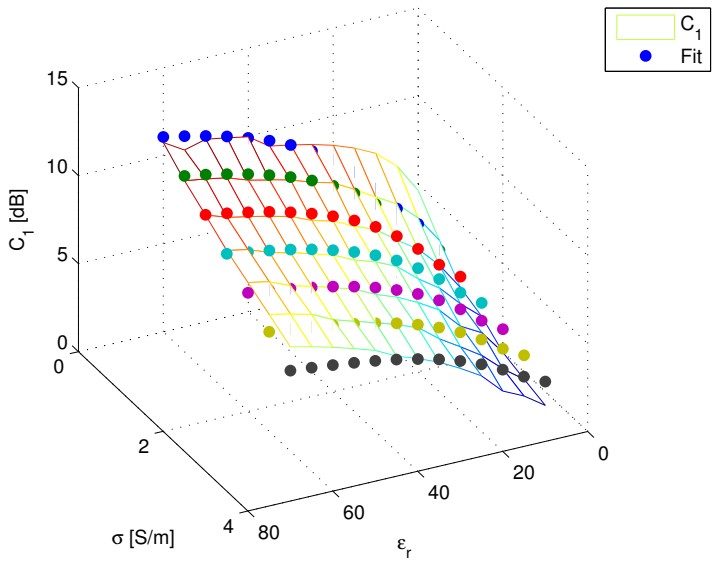

Fig. 11. $C_1|_{\mathrm{dB}}$ as a function of both ϵ_r and σ.

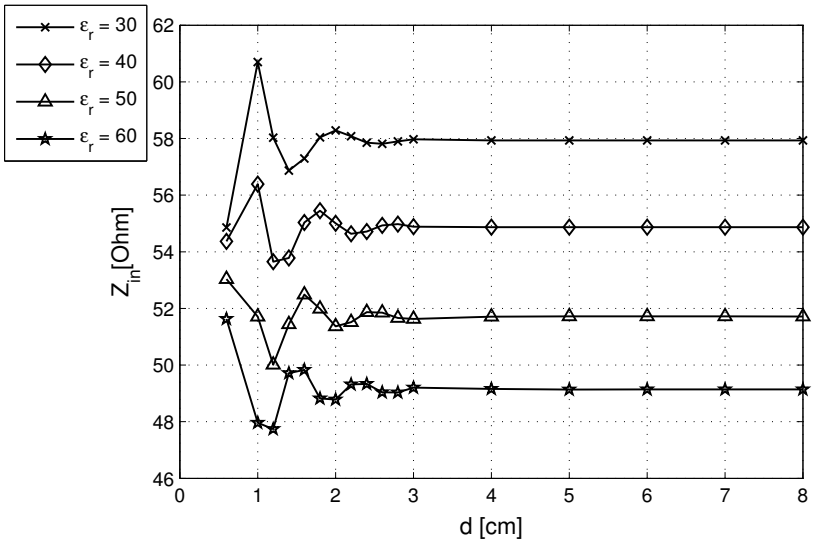

Fig. 12. Input impedance $|Z_{in}|$ vs. distance d for different ϵ_r (σ = 2 S/m).

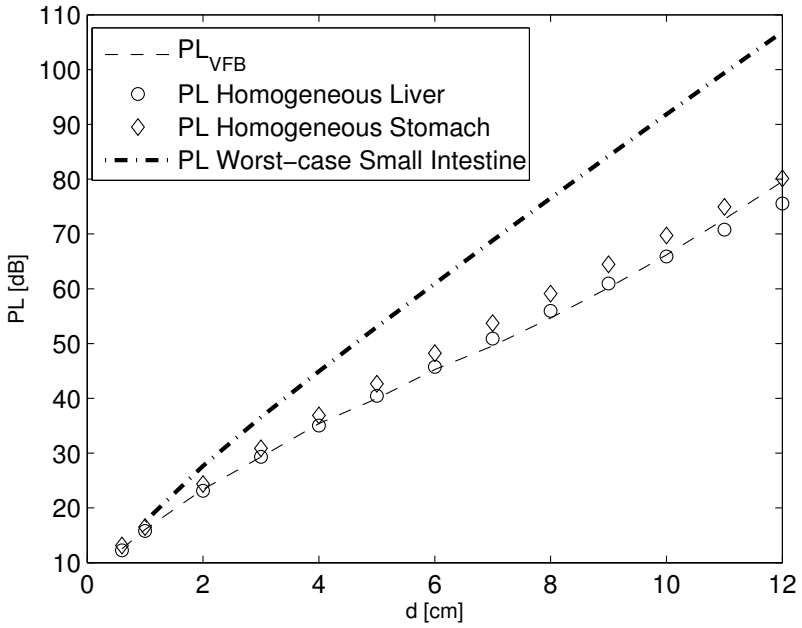

Fig. 13. PL in the male child model (heterogeneous model) for a separation of the Tx and the Rx up to 12 cm and PL in homogeneous medium of stomach and liver and PL for worst tissue property.